

Chapter 4

Local Hyperbolic/Kinetic Systems in 1D



4.1 Introduction

The models discussed in Chap. 3 assumed that individuals can move in only one direction, either left or right, depending on the sign of the velocity. Of course, the individual's velocity can be density-dependent and change its sign as time progresses, leading to changes in the movement direction of the whole population. However, recent approaches in experimental ecology have started to focus on collecting data on the speed and turning rates of different animals exhibiting collective behaviours [1–3]. Similarly, studies in cell biology have started to investigate the individual movement of cells and bacteria, some of which exhibit for example “run-and-turn” behaviours [4]. These behaviours are similar to the “run-and-tumble” and “run-reverse-turn” behaviours in bacterial communities [5, 6]; see also Fig. 4.1a–c. While the turning events of bacteria are usually random, the turning events of amoebae cells can exhibit short-term memory with cells having a tendency of turning away from previous turns [4]; see also Fig. 4.1d. The running speeds, turning rates and turning angles during changes in movement direction of cells and bacteria can all be measured experimentally [2, 4, 5], thus allowing for a better quantitative description of cell/bacterial/animal movement. However, when cells/bacteria/animals interact with conspecifics within a community [7], they might change their velocity and turning in response to the behaviour of their conspecifics. This adds another layer of complexity to the dynamics of the whole system, as individual cell/bacteria/animal behaviours are difficult to predict emergent group-level behaviours.

A different type of transport phenomena occurs in cellular biology, during the bidirectional movement of molecules/particles along polarised microtubules or axons [10–12] (see also Fig. 4.2). These particles (e.g., mitochondria, pigment granules, lipid droplets, viruses [13]) are transported with the help of molecular motors such as cytoplasmic dynein and conventional kinesin. Usually the kinesin

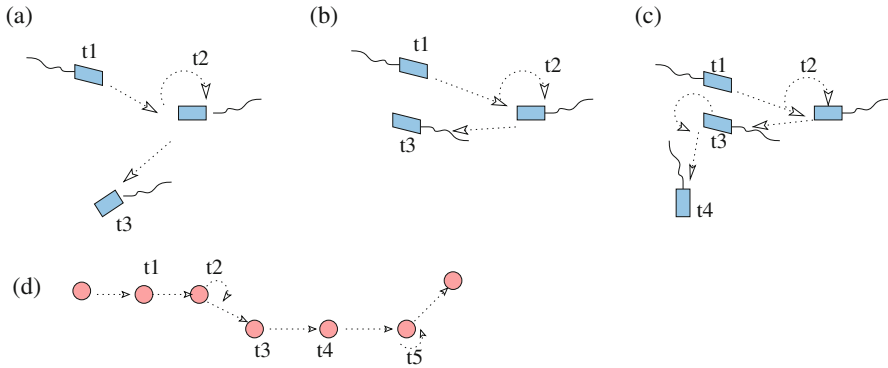


Fig. 4.1 Caricature description of three different bacterial movement strategies, and one cell movement strategy. **(a)** The “run-and-tumble” strategy, where the turning angle during the “tumble” is random. This strategy has been observed, for example, in *Escherichia coli*, *Salmonella typhimurium*, *Bacillus subtilis* [8]; **(b)** The “run-and-reverse” strategy, where the bacteria undergo a 180° reorientation. This strategy has been observed, for example, in *Shewanella putrefaciens*, *Pseudoalteromonas haloplanktis* and *Deleya marina* [8]; **(c)** The “run-reverse-flick” strategy, which combines the run-and-reverse with a random and fast tumble described by the flick. This strategy has been observed in *Vibrio Alginolyticus* [8, 9] or in *Pseudomonas aeruginosa* [5]. **(d)** The “run-and-turn” strategy exhibited by crawling cells [4], which is similar to the run-and-tumble strategy in bacteria. Note the tendency of cells to reverse the turning direction from one step to another (as emphasised in time steps t_2 and t_5)

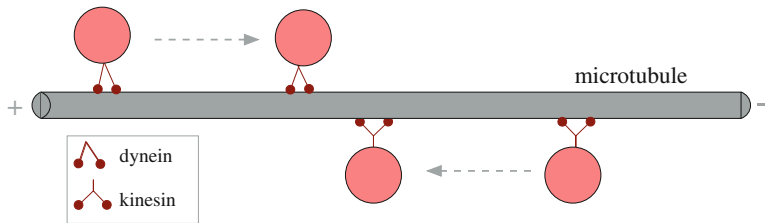


Fig. 4.2 Caricature description of bidirectional movement of particles along a microtubule filament (or axon), which displays polarity (see the “+” and “-” signs at the end of the microtubule). The transported particles are bound to (and transported along) the microtubule by molecular motors such as dynein and kinesin

moves to the microtubules’ “+” end, while the dynein moves to the “-” end [12, 13]. Since many molecules have both types of motors, it has been suggested that the actual transport could be the results of a “tug-of-war” between molecular motors for the “+” and “-” directions, with a “pause” state being reached when a particle has activated both types of motors [12]. The transported particles can reverse their direction every few seconds, depending on the motors that dominate the dynamics [12, 13]. This movement-turning behaviour (towards the $+/-$ ends of the microtubules) gives rise to a biased random walk, which characterises the transport

of fish and frog pigment granules inside cells, or the transport of adenoviruses and herpes viruses through the cytoplasm [13].

It should be mentioned that bi-directional movement has also been observed in various ecological contexts: e.g., during ants movement along pheromone trails [14], or during pedestrian movement at crosswalks [15] or along corridors [16].

To be able to incorporate the directionality of movement into the 1D mathematical models for self-organised biological behaviours (to further investigate emergent group-level phenomena, also by using available experimental data), one can split the initial population (u) into two subpopulations of left-moving (u^-) and right-moving (u^+) individuals (or cells/bacteria/etc.). This leads to systems of equations describing the movement and interactions of left-moving and right-moving individuals as they change their direction of travel and/or their speeds. Because these models incorporate detailed individual-level information regarding movement directions (left or right), they are in fact kinetic (i.e. mesoscale) models, being often referred to as “two-speed kinetic models”.

In the following, we review briefly some hyperbolic systems derived to investigate the movement of organisms in response to local conspecifics. We start with the simplest hyperbolic models, which assume that left-moving and right-moving individuals travel at a constant speed and have constant turning rates. Since these models could not explain the complexities of some observed biological aggregations (e.g., the splitting and merging of groups, or the increase in population size), more complicated models have been derived. These new models incorporate density-dependent turning rates, density-dependent speeds, or reaction terms describing population growth and decay. Throughout this section, the underlying assumption is that the behaviour of individuals is influenced only by the local density of their conspecifics.

As for the one-population models in Chap. 3, one can use a variety of simple first order and higher order finite difference schemes or finite volume schemes to discretise and simulate the solutions of these hyperbolic systems. Since the numerical approaches are similar to those mentioned in Sect. 3.8, we will not discuss them here again. However, for a more detailed discussion of these various numerical schemes, see Chap. 7.

4.2 Derivation of Local Models in 1D

The derivation of local hyperbolic models for self-organised movement follows the classical Goldstein-Kac theory for correlated random walk [17, 18]. This approach has been reviewed, for example, in [19–21]. In brief, denote by $u^+(x, t) \in \mathbb{R}$ and $u^-(x, t) \in \mathbb{R}$ the densities of right-moving and left-moving individuals at position $x \in \mathbb{R}$ and time $t \in \mathbb{R}^+$. To derive the equations describing the evolution of these densities, let us first consider the behaviour of an individual organisms (in a population of size N). Denote by $p^+(x, t)$ ($p^-(x, t)$) the probability that a randomly chosen right-moving (left-moving) individual is found inside the interval

$[x - \Delta x/2, x + \Delta x/2]$ at time t . These probabilities are defined as follows [22, 23]:

$$p^\pm(x, t) = \frac{1}{N} \int_{x-\Delta x/2}^{x+\Delta x/2} u^\pm(s, t) ds \longrightarrow \frac{\Delta x u^\pm(x, t)}{N} \text{ when } \Delta x \rightarrow 0. \quad (4.1)$$

We denote by Δx and Δt the space and time steps, respectively. At each time step, the individual changes direction with probability $\lambda^+ \Delta t$ (if it was initially moving right) or $\lambda^- \Delta t$ (if it was initially moving left); see also Fig. 4.3. This leads to the following *master equations*:

$$p^+(x, t + \Delta t) = (1 - \lambda^+ \Delta t) p^+(x - \Delta x, t) + (\lambda^- \Delta t) p^-(x + \Delta x, t), \quad (4.2a)$$

$$p^-(x, t + \Delta t) = (\lambda^+ \Delta t) p^+(x - \Delta x, t) + (1 - \lambda^- \Delta t) p^-(x + \Delta x, t). \quad (4.2b)$$

Expanding Eqs. (4.2) in Taylor series, taking the limits $\Delta t, \Delta x \rightarrow 0$, such that $\gamma = \Delta x/\Delta t$, and using (4.1), leads to the following hyperbolic equations for the evolution of densities of right- and left-moving individuals:

$$\frac{\partial u^+}{\partial t} + \gamma \frac{\partial u^+}{\partial x} = -\lambda^+ u^+ + \lambda^- u^-, \quad (4.3a)$$

$$\frac{\partial u^-}{\partial t} - \gamma \frac{\partial u^-}{\partial x} = \lambda^+ u^+ - \lambda^- u^-. \quad (4.3b)$$

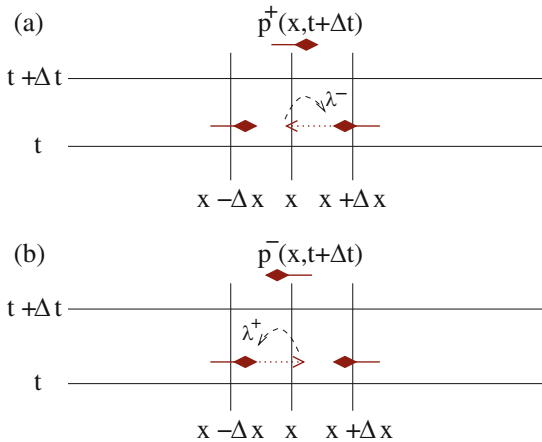


Fig. 4.3 The movement and turning behaviour of (a) a right-moving individual, and (b) a left-moving individual, in response to *local neighbours*. A right-moving individual can be positioned at x at time $t + \Delta t$, if at the previous time step t it was at $x - \Delta x$ and kept moving in the same direction, or it was at $x + \Delta x$ and moving left, and changed direction at the end of the time step Δt . A similar explanation holds for the movement of a left-moving individual (see (b)). The change in direction occurs at rates λ^\pm

Here, λ^\pm are the constant turning rates, and γ is the constant speed. Note that Eq. (4.1) helps us connect the random movement of an individual (given by the position probabilities $p^\pm(x, t)$) to the population distribution (described by the density functions $u^\pm(x, t)$).

Remark 4.1 As mentioned above, models (4.3) are often referred to as “two-speed kinetic models”, since they incorporate individual-level characteristics (left and right velocities $\pm\gamma$, and turning probabilities λ^\pm) into the description of population variables. For example, we could have defined $u^\pm(x, t) := u^\pm(x, t; \pm\gamma)$, to make it more clear that the population densities depend on the discrete speeds $\pm\gamma$. We will return to this aspect in Chap. 6, in the context of 2D kinetic Boltzmann-type equations that can be reduced in 1D to equations similar to (4.3), by assuming that the direction angle ϕ can take only two values, $\pm\pi$ (which reduces the continuous speed/orientation model to a discrete speed/orientation model).

The hyperbolic system (4.3) can be reduced to a 1D telegraph equation by considering the total population density $u = u^+ + u^-$ and the population flow $v = u^+ - u^-$. These two variables satisfy the following equations

$$\frac{\partial u}{\partial t} + \gamma \frac{\partial v}{\partial x} = 0, \quad (4.4a)$$

$$\frac{\partial v}{\partial t} + \gamma \frac{\partial u}{\partial x} = \Lambda_1 u - \Lambda_2 v. \quad (4.4b)$$

Here, $\Lambda_1 = \lambda^- - \lambda^+$ and $\Lambda_2 = \lambda^- + \lambda^+$. Differentiating Eqs. (4.4) with respect to x and t , and eliminating the derivatives $\frac{\partial^2 v}{\partial t \partial x}$ and $\frac{\partial v}{\partial x}$ (a process known as the Kac trick [18]) leads to the following telegraph equation:

$$\frac{\partial^2 u}{\partial t^2} + \Lambda_2 \frac{\partial u}{\partial t} = \gamma^2 \frac{\partial^2 u}{\partial x^2} - \gamma \Lambda_1 \frac{\partial u}{\partial x}. \quad (4.5)$$

A similar equation (with no drift $\Lambda_1 = 0$ and with a reaction term) was investigated by Holmes [19] in the context of population dispersal. Holmes [19] showed that this telegraph equation can predict dispersal patterns that are very similar to the ones obtained with parabolic equations.

Remark 4.2 Parabolic equations can be obtained as a limit of Eqs. (4.3), following a rescale of the speed and turning rates: $\gamma = \gamma_0/\epsilon$, $\lambda^\pm = \lambda_0/\epsilon^2$ (i.e., individuals travel extremely fast and turn very rapidly), or equivalently a rescale of the space and time variables: $x = x^*/\epsilon$, $t = t^*/\epsilon^2$. The limit $\epsilon \rightarrow 0$ applied in the context of the previous rescaling is known as the *parabolic limit*.

Remark 4.3 Hyperbolic equations of the form (2.1) (with $R(u) = 0$) can be obtained as a limit of these two-speed kinetic equations (4.3), following a slightly different rescaling: $x = x^*/\epsilon$, $t = t^*/\epsilon$. The limit $\epsilon \rightarrow 0$ applied in the context of the previous rescaling is known as the *hydrodynamic limit*.

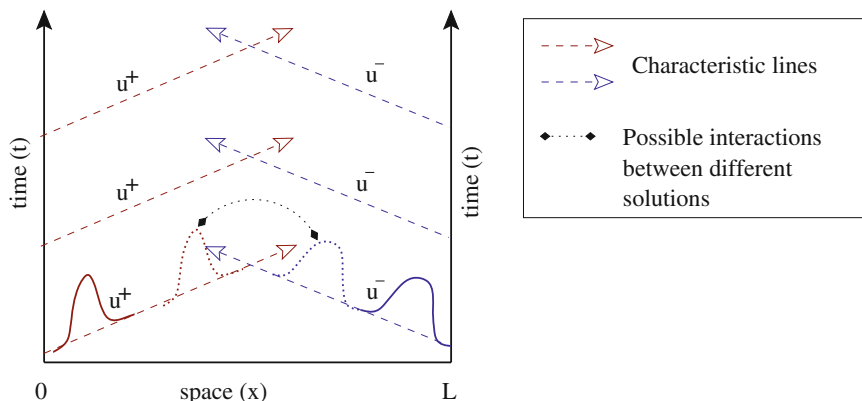


Fig. 4.4 Solutions of hyperbolic systems transported along characteristic lines, on a finite domain $[0, L]$. If the left-moving and right-moving solutions do not interact with each other, they maintain their shapes until they reach the other end of the domain. Otherwise, the left-moving and right-moving solutions might change their shapes following interactions with each other

Since the majority of biological populations live in restricted areas, the mathematical models that investigate these populations are usually defined on finite domains $[0, L]$. For hyperbolic systems, the solutions are transported along the characteristic lines, and thus the boundary conditions have to be prescribed only at the points where the characteristics are directed inward [20] (see also Fig. 4.4). Briefly, the three biologically realistic boundary conditions are: Dirichlet conditions (for domains on which the population density is known at the boundary; including the case where populations vanish on the boundaries), Neumann conditions (for closed domains where no individuals/cells/particles can leave) and periodic boundary conditions (for ring domains, or approximations of infinite domains). A detailed discussion of these boundary conditions and their role on the existence of weak and classical solutions for system (4.3) can be found in [20, 24]. Similar boundary conditions can be derived for the corresponding telegraph equations that model population movement [20]. We will return to these boundary conditions in Sect. 7.3, in the context of numerical simulations for kinetic and hyperbolic systems.

In the following, we discuss briefly a few examples of hyperbolic models that have been derived to investigate interactions between prey and predators moving in opposite directions [25], or the formation and movement of bacterial aggregations, such as colonies of *Myxobacteria* [26], colonies of *Dictyostelium discoideum* [27], or even the intracellular active transport of particles along microtubules [28]. While many of these models consider constant speeds and turning rates, a few others consider turning rates and speeds that are influenced by conspecifics (either directly through their density, or indirectly through chemical signals produced by these conspecifics). We will also discuss a few examples of models that have different reaction terms (i.e., the right-hand-sides of Eqs. (4.3) do not contain only transition terms between the left-moving/right-moving states, but also transitions between

moving/stationary states, as well as birth/death processes). Although we discuss separately models with density-dependent speeds, density-dependent turning rates, reaction terms, multiple-population models, as well as first and second order traffic models, we need to emphasise that many of these models can fall into multiple categories (e.g., could have density-dependent speeds and reaction terms, or could be traffic-like models with multiple populations). Also, while a few models are described exclusively by transport and/or reaction-transport equations, other models combine reaction-transport equations with parabolic equations or ordinary differential equations.

4.3 Density-Dependent Turning Rates

Model (4.3) describes the movement of right-moving and left-moving individuals when their turning rates (λ^\pm) are constant. While this assumption is supported by experimental data on individual cells, bacteria or animals [1–3], it does not tell the whole story since individuals in a group can also turn in response to interactions with their neighbours. These interactions can be direct [25, 26, 29], or indirect through chemicals produced by these neighbours [27, 30].

For the hyperbolic models (4.3) with constant speed and very simple density-dependent turning rates (e.g., $\lambda^+(u^+, u^-) = 0$ and $\lambda^-(u^+, u^-) = u^+$ as in [25]), it is possible to find exact analytical solutions. For more general models, however, only numerical and analytical methods (such as existence and asymptotic results) could be used to investigate the various types of solutions. For example, Lutscher and Stevens [26] studied the rippling behaviour observed in *Myxobacteria* colonies. The hyperbolic model that they used incorporated turning rates that have a constant random component (μ) and a directed density-dependent component (μ^\pm): $\lambda^\pm = \mu + \mu^\pm(u^+, u^-)$, with $\mu^\pm(u^+, u^-) = 2 \tanh u^- \sqrt{u^-}$ or $\mu^\pm(u^+, u^-) = \frac{3}{1+(u^++u^-)^3}(u^-)^2$. First, the authors showed the existence of unique solutions (in \mathbb{C}^1) for the local hyperbolic system introduced in [26]. (Note that the proof used a contraction argument; see also Chap. 8.) Then, using analytical and numerical results, they investigated the role of these nonlinear turning functions μ^\pm on the overall group patterns. For the numerical results, the authors used a first-order upwind scheme with periodic boundary conditions, as well as a second-order Lax-Wendroff scheme. The results showed that when the turning functions are equal and depend only on the individuals moving in the opposite direction (see the $\mu^\pm(u^+, u^-)$ functions above), the model exhibits ripples and moving aggregations (travelling pulses). These two patterns are shown in Fig. 4.5; see also Table 1.2 for a description of these patterns.

Very recently, Kang et al. [31] identified parameter regions of global existence for ripples and waves, and parameter regions of existence of finite-time blow-up patterns, in a local hyperbolic model with density-dependent turning rates. The authors used the same model (4.3) with the turning rates given by $\lambda^+(u^+, u^-) =$

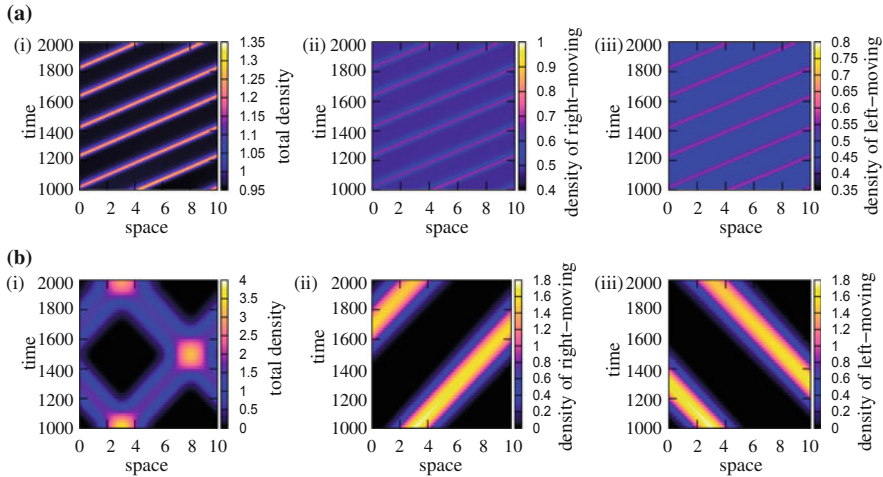


Fig. 4.5 Reproduction of spatio-temporal patterns observed in [26] for a hyperbolic system of the form (4.3) with constant speed γ and turning rates $\lambda^\pm = \mu + 2 \tanh u^- \sqrt{u^-}$. **(a)** travelling pulses (or waves); **(b)** ripples (or standing waves). Panels (i) show the total population density $u = u^+ + u^-$; panels (ii) show the density of right-moving subpopulation u^+ ; panels (iii) show the density of left-moving subpopulation u^-

$g(u^-)$ and $\lambda^-(u^+, u^-) = g(u^+)$, where

$$g(u) = \mu + \frac{u^p}{1 + \nu u^q}, \quad \text{for } u \in \mathbb{R}^+. \quad (4.6)$$

As before, μ is a constant spontaneous reversal rate. Parameter p is a rate of reversal increase for small population densities, while parameter $p - q$ is a rate of reversal increase/decrease for large population densities [31]. Finally, ν describes a saturation level where the reversal rates stop increasing at the same rates as for small populations [31]. For specific values of p , q , and μ the authors have shown the existence of nontrivial wave patterns when $\nu \in (0, 1/8) \cup \{0\}$, existence of finite-time blow-up solutions for $\nu = 0$, and stable spatially homogeneous (or equidistributed [31]) steady states for $\nu \in [1/8, \infty)$.

We note that the rippling patterns obtained by Lutscher and Stevens [26], Kang et al. [31] occurred when individuals changed their movement direction only in response to conspecific moving in the opposite direction. Actually, this biological mechanism seems to be crucial for the formation of ripples, as observed in discrete models [32, 33], parabolic models [34–36], as well as nonlocal hyperbolic models [37]. (We will revisit this pattern in Chap. 5.) Mathematically, it was shown that the formation of ripples is associated with Hopf bifurcations [26]. For a review of these bifurcations see the discussion in Chap. 8.

In contrast to these hyperbolic models where the turning rates depend on the local density of conspecifics, Hillen and Stevens [27] derived a slightly different model to investigate the effect of indirect interactions among organisms. These interactions

were mediated by an external signal S , which was produced by individuals at a rate α , decayed at a rate β , and diffused into the environment at a rate D :

$$\frac{\partial u^+}{\partial t} + \gamma \frac{\partial u^+}{\partial x} = -\lambda^+ \left(S, \frac{\partial S}{\partial x} \right) u^+ + \lambda^- \left(S, \frac{\partial S}{\partial x} \right) u^-, \quad (4.7a)$$

$$\frac{\partial u^-}{\partial t} - \gamma \frac{\partial u^-}{\partial x} = \lambda^+ \left(S, \frac{\partial S}{\partial x} \right) u^+ - \lambda^- \left(S, \frac{\partial S}{\partial x} \right) u^-, \quad (4.7b)$$

$$\tau \frac{\partial S}{\partial t} = D \frac{\partial^2 S}{\partial x^2} + f(S, u^+ + u^-). \quad (4.7c)$$

Here, function $f(S, u^+ + u^-) = -\beta S + \alpha(u^+ + u^-)$ describes the production/decay of signal S . Moreover, the turning rates depend not only on the signal alone but also on the gradient of this signal ($\partial S/\partial x$), suggesting some long-distance interactions. Focusing on existence (and uniqueness) results, the authors showed that solutions exist globally (i.e., there are no blow-up solutions) when signal production is linear (i.e., $f(S, u^+ + u^-) = \alpha(u^+ + u^-)$) and the turning rates ($\lambda^\pm(S, \partial S/\partial x)$) are bounded. However, blow-up solutions are possible when the production of signal S is nonlinear (i.e., $f(S, u^+ + u^-) = S(u^+ + u^-)$). Hillen and Levine [38] investigated a similar hyperbolic model and showed that for their case, the formation of blow-up patterns is preceded by the turning rates becoming negative. This causes the densities u^\pm to become negative, meaning that the hyperbolic model becomes unrealistic just before the blow-up [38]. Even if these density blow-up patterns are not biologically realistic, they can indicate that the investigated organisms tend to form very dense aggregations. Examples of blow-up solutions are shown in Figs. 1.10 and 5.22, and discussed in Table 1.2.

Note that these hyperbolic systems could be seen as displaying another type of pattern: spatially homogeneous solutions with the majority of individuals aligned in one direction. Since individuals are spread over the entire domain, they do not actually form heterogeneous patterns. However, because the population can split into two subpopulations of left-moving and right-moving individuals, this splitting this could be seen as a type of group pattern. When the majority of individuals are moving in one direction, this pattern is the precursor of lane patterns observed in some 2D models [39]; see also Fig. 1.11.

4.4 Analytical Approaches for the Investigation of Patterns: Stability of Homogeneous States and Travelling Waves for Models with Density-Dependent Turning Rates

In the following we focus on a simple local hyperbolic model introduced by Lutscher [29] to describe the alignment of animals in one spatial dimension, and discuss the stability of spatially homogeneous steady states and the stability of

waves of perfect alignment (i.e., all individuals are aligned in one direction, causing the second population to become zero; which is in contrast to the case depicted in Fig. 4.5a, where the second population persists at some very low densities). The model takes the form [29]

$$\frac{\partial u^+}{\partial t} + \gamma \frac{\partial u^+}{\partial x} = \mu(u^+, u^-)(u^+ - u^-), \tag{4.8a}$$

$$\frac{\partial u^-}{\partial t} - \gamma \frac{\partial u^-}{\partial x} = \mu(u^+, u^-)(u^- - u^+), \tag{4.8b}$$

with

$$\mu(u^+, u^-) = \frac{a}{(u^+ + u^-)^3} u^+ u^- - \frac{\mu_*}{2}. \tag{4.9}$$

The first term in the above equation is a density-dependent turning rate (with $a > 0$) that leads to alignment, while the second term (with $\mu_* \geq 0$) is a constant random tuning rate. It is clear from Eqs. (4.8) that this model can have spatially homogeneous steady states with $u^+ = u^- = \bar{u}$, or states with $u^+ \neq u^-$ (that satisfy $\mu(u^+, u^-) = 0$); see Fig. 4.6. It was shown in [29] that small spatial perturbations of spatially homogeneous steady states $u^\pm(x, t) = \bar{u}$ (i.e., $u^\pm = \bar{u} + c_\pm e^{\sigma t + i k x}$, with $0 < c_\pm \ll 1$) lead to a dispersion relation with eigenvalues given by:

$$\sigma_{1,2} = \left(\frac{a}{4}\bar{u}^2 - \frac{\mu_*}{2}\right) \pm \frac{1}{2}\sqrt{\left(\frac{a}{4}\bar{u}^2 - \frac{\mu_*}{2}\right)^2 - 4\gamma^2 k^2}. \tag{4.10}$$

When μ_* is large, $Re(\sigma_{1,2}) < 0$ and all modes are stable. However, as we decrease μ_* below a critical threshold $\mu_* = a\bar{u}^2/2$ all modes become unstable; see Fig. 4.7. (Note that similar dispersion relations, where eigenvalues can be unstable for an

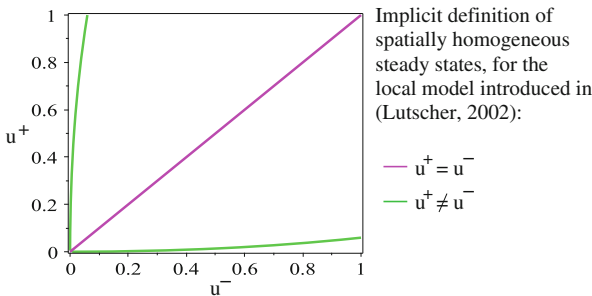


Fig. 4.6 Examples of spatially homogeneous steady states (i.e., states which satisfy $\partial u^\pm/\partial t = \partial u^\pm/\partial x = 0$) in the (u^+, u^-) plane, for the local hyperbolic model (4.8). One can have states with $u^+ = u^-$ (magenta line), or states with $u^+ \neq u^-$ (green curve). Note the symmetry of the steady states with respect to the $u^+ \leftrightarrow u^-$ interchange

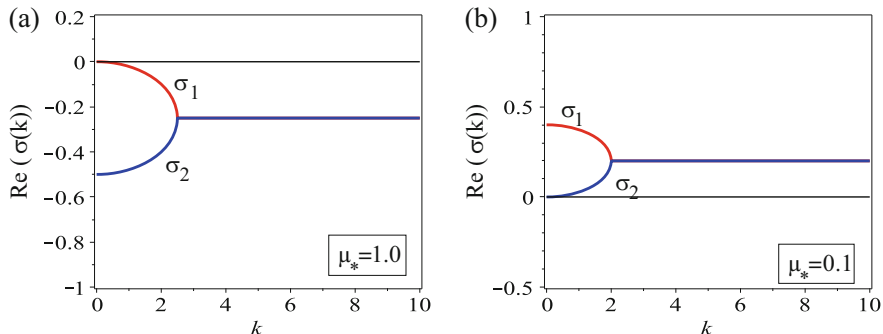


Fig. 4.7 Real part of the dispersion relation as given by (4.10); the red curves describe σ_1 , while the blue curves describe σ_2 . Note that (a) for large μ_* (e.g., $\mu_* = 1.0$) all wavenumbers k are stable, while (b) for small μ_* (e.g., $\mu_* = 0.1$) all wavenumbers k are unstable

infinite range of wavenumbers, have been shown to exist in a relatively similar local hyperbolic system introduced in [40].) This spectral result impacts the existence of a centre manifold reduction—as it will be discussed in Chap. 8.

Lutscher [29] also showed that simple waves of total alignment (i.e., waves of the form $u^+(x, t) = u_0^+(x - \gamma t)$ and $u^-(x, t) = 0$, or $u^+(x, t) = 0$ and $u^-(x, t) = u_0^-(x + \gamma t)$) are linearly stable with respect to the positive cone. To this end, the author assumed that $u^+ \geq 0$ and $u^- = 0$, and applied small perturbations w^\pm . These perturbations satisfy the following linearised system:

$$\begin{aligned} \frac{\partial w^+}{\partial t} + \gamma \frac{\partial w^+}{\partial x} &= a(u)(u^+)^2 w^-, \\ \frac{\partial w^-}{\partial t} - \gamma \frac{\partial w^-}{\partial x} &= -a(u)(u^+)^2 w^-. \end{aligned} \quad (4.11)$$

Since the second equation (for w^-) decouples from the first equation, one can integrate it to obtain

$$\frac{d}{dt} \int_D w^-(x, t) dx = - \int_D a(u) u^+(x, t)^2 w^-(x, t) dx \leq 0, \quad (4.12)$$

which implies that w^- converges to 0, and thus the simple wave ($u^+ > 0$, $u^- = 0$) is stable.

To conclude the discussion of the model in [29] we note that the author also showed that for all initial data $u_0^\pm \in \mathbb{L}^\infty(\mathbb{R})$ there exists a unique mild solution (see definition below) $u^\pm \in \mathbb{L}^\infty(\mathbb{R} \times [0, T])$ of the initial value problem, for some $T > 0$. Moreover, if the initial data is in $C^k(\mathbb{R})$ then all solutions are in $C^k(\mathbb{R})$ provided that $\mu \in C^{k,1}$. The proof of this existence result uses a standard contraction argument [29] (see also Chap. 8).

Definition 4.1 A *mild solution* is a pair of functions $(u^+, u^-) \in \mathbb{L}^\infty(\mathbb{R} \times [0, T])^2$ that satisfies the following integral equation (obtained by integrating system (4.8) along the characteristic lines $x \pm \gamma t = \text{const}$ and using a new variable $z = z_0 \pm \gamma t$):

$$u^\pm(z) = u_0^\pm \pm \int_{z_0}^z \mu(u^+, u^-)(u^+ - u^-)(y)dy. \quad (4.13)$$

4.5 Density-Dependent Speeds

The models mentioned in the previous section assume that the speed is constant, while the turning behaviour is the result of local alignment interactions. However, it is well known that some organisms change also their speed in response to interactions with neighbours [41]. This can lead to an additional equation for the evolution of the speed.

One of the first generalisations of models (3.1) to two different populations u and v (or “two-phase” models) was proposed by Bick and Newell [42] in the context of two-lane traffic:

$$\frac{\partial u}{\partial t} + \frac{\partial}{\partial x} (u(1 - u - \beta v)) = 0, \quad (4.14a)$$

$$\frac{\partial v}{\partial t} + \frac{\partial}{\partial x} (-v(1 - \beta u - v)) = 0. \quad (4.14b)$$

Here, $\beta > 0$ models the changes in the velocities of the two populations as a result of their interactions. The authors then investigated analytically the possibility of having shock curves that connect different states.

Chertock et al. [43] derived a local hyperbolic model for pedestrian movement from a microscopic model on a lattice. The authors considered the probabilities of left-moving ($p_x^-(t)$) and right-moving ($p_x^+(t)$) pedestrians to be in a lattice cell x at time t , and defined four different velocities which depend on the presence or absence of pedestrians in the adjacent lattice cells (at $x \pm \Delta x$). For example, if right-moving pedestrians are found in a cell x (i.e., $p_x^+ = 1$, but $p_{x+\Delta x}^+ = 0$), then their velocities depend on the presence/absence of left-moving pedestrians:

1. velocity= c_0 if $p_x^- = p_{x+\Delta x}^- = 0$ (no left-moving pedestrians in cells at x or $x + \Delta x$),
2. velocity= c_1 if $p_x^- = 1$, $p_{x+\Delta x}^- = 0$ (left-moving pedestrians in the cell at x),
3. velocity= c_2 if $p_x^- = 0$, $p_{x+\Delta x}^- = 1$ (left-moving pedestrians in the cell at $x + \Delta x$),
4. velocity= c_3 if $p_x^- = p_{x+\Delta x}^- = 1$ (left-moving pedestrians in cells at x and $x + \Delta x$),

with $c_3 < c_2 \approx c_1 < c_0$. Similar velocities can be defined for left-moving pedestrians when $p_x^- = 1$ (and their velocities depend on the presence/absence of

right-moving pedestrians). With these definitions, the probabilities of moving from cell x to cell $x + \Delta x$ (for p_x^+) or from cell x to cell $x - \Delta x$ (for p_x^-) in one time step Δt are

$$\begin{aligned} P_{x \rightarrow x+\Delta x}^+ &= \Delta t \left(c_0 p_x^+ (1 - p_{x+\Delta x}^+) (1 - p_x^-) (1 - p_{x+\Delta x}^-) \right. \\ &\quad + c_1 p_x^+ (1 - p_{x+\Delta x}^+) p_x^- (1 - p_{x+\Delta x}^-) \\ &\quad + c_2 p_x^+ (1 - p_{x+\Delta x}^+) (1 - p_x^-) p_{x+\Delta x}^- \\ &\quad \left. + c_3 p_x^+ (1 - p_{x+\Delta x}^+) p_x^- p_{x+\Delta x}^- \right), \end{aligned} \quad (4.15a)$$

$$\begin{aligned} P_{x \rightarrow x-\Delta x}^- &= \Delta t \left(c_0 p_x^- (1 - p_{x-\Delta x}^-) (1 - p_x^+) (1 - p_{x-\Delta x}^+) \right. \\ &\quad + c_1 p_x^- (1 - p_{x-\Delta x}^-) p_x^+ (1 - p_{x-\Delta x}^+) \\ &\quad + c_2 p_x^- (1 - p_{x-\Delta x}^-) (1 - p_x^+) p_{x-\Delta x}^+ \\ &\quad \left. + c_3 p_x^- (1 - p_{x-\Delta x}^-) p_x^+ p_{x-\Delta x}^+ \right). \end{aligned} \quad (4.15b)$$

In the limit $\Delta x, \Delta t \rightarrow 0$, this microscale model becomes the following macroscale model:

$$\frac{\partial u^+}{\partial t} + \frac{\partial}{\partial x} \left(f(u^+) g(u^-) \right) = 0, \quad (4.16a)$$

$$\frac{\partial u^-}{\partial t} - \frac{\partial}{\partial x} \left(f(u^-) g(u^+) \right) = 0, \quad (4.16b)$$

with

$$f(w) = w(1-w), \quad g(w) = (c_3 - c_2 - c_1 + c_0)w^2 + (c_2 + c_1 - 2c_0)w + c_0. \quad (4.17)$$

The authors used numerical simulations to compare the dynamics of the microscale and macroscale models. For the simulation of the macroscopic model, they employed a semi-discrete, second-order, central-upwind scheme [44], with a nonlinear ‘‘minmod’’ limiter to avoid oscillations in the reconstruction of the solution (see a description of this limiter in Chap. 7). The simulations showed that both models could exhibit rippling behaviour, with pulses of left- and right-moving pedestrians passing through each other. The strength of the slow-down interactions (which is determined by the values of the velocities c_j , $j = 0, 1, 2, 3$) determines how well the numerics for the microscopic model match the numerics for the macroscopic model: lower slow-down interactions are associated with an almost perfect match. Model (4.16)–(4.17) can be non-hyperbolic in some regions of the parameter space, since the Jacobian matrix

$$J = \begin{pmatrix} f'(u^+)g(u^-) & f(u^+)g'(u^-) \\ -f'(u^-)g'(u^+) & -f'(u^-)g(u^+) \end{pmatrix} \quad (4.18)$$

has real eigenvalues (which ensures hyperbolicity) only if the following condition holds true:

$$\left(f'(u^-)g(u^+) + f'(u^+)g(u^-) \right)^2 - 4f(u^-)f(u^+)g'(u^-)g'(u^+) > 0.$$

Hence it is possible to have a non-hyperbolic regime for some specific values of c_0 , c_1 , c_2 and c_3 , for which the above inequality does not hold (and this happens when the left-moving and right-moving pedestrians were both present at a particular location in space). In this regime, the solution of the model (4.16) was shown to exhibit spurious oscillations. To address this numerical problem, the authors considered also a diffusive correction which described the presence of pedestrians moving in the opposite directions:

$$\frac{\partial u^+}{\partial t} + \frac{\partial}{\partial x} \left(f(u^+)g(u^-) \right) = \frac{\epsilon}{2} \frac{\partial}{\partial x} \left(g(u^-) \frac{\partial u^+}{\partial x} \right), \quad (4.19a)$$

$$\frac{\partial u^-}{\partial t} - \frac{\partial}{\partial x} \left(f(u^-)g(u^+) \right) = \frac{\epsilon}{2} \frac{\partial}{\partial x} \left(g(u^+) \frac{\partial u^-}{\partial x} \right), \quad (4.19b)$$

Numerical simulations for this new model showed solutions corresponding to rarefaction waves and stop-and-go behaviours in pedestrian dynamics [43]; see also Fig. 1.10b.

Model (4.16) can be generalised to include a desired pedestrian velocity V . Appert-Rolland et al. [45] proposed a model for two-way one-lane pedestrian traffic which assumes that pedestrians adapt their speed in response to pressure from their neighbours:

$$\frac{\partial u^+}{\partial t} + \frac{\partial}{\partial x} \left(u^+(V - p(u^+, u^-)) \right) = 0, \quad (4.20a)$$

$$\frac{\partial u^-}{\partial t} - \frac{\partial}{\partial x} \left(u^-(V - p(u^+, u^-)) \right) = 0. \quad (4.20b)$$

Here, function p is an increasing function of both u^+ and u^- . Generally, p can be obtained from the data. However, in [45], the authors propose a particular form for function p that allows for the investigation of congestion effects (see also Eqs. (3.18)):

$$p(u^+, u^-) = p^\epsilon(u^+, u^-) = P(u^+ + u^-) + Q^\epsilon(u^+, u^-), \quad (4.21a)$$

$$P(u^+ + u^-) = M(u^+ + u^-)^m, \quad m \geq 1, \quad (4.21b)$$

$$Q^\epsilon(u^+, u^-) = \frac{\epsilon}{q(u^+) \left(\frac{1}{u^+ + u^-} - \frac{1}{u^*} \right)^d}, \quad d > 1, \quad (4.21c)$$

with q an increasing function. Here, congestion occurs when $u^+ + u^- \rightarrow u^*$. Note that also for this model there are regions in the parameter space where (4.20) is non-hyperbolic. As for the previous example, the authors considered a diffusive perturbation of the model to stabilise the large wavenumbers that arise in the parameter region where the model is non-hyperbolic. The numerical simulations (performed with a central difference scheme [46]) have shown the existence of travelling pulses, where both subpopulations u^\pm travel in the same direction. For large diffusive perturbations, the dynamics of the system approaches a spatially homogenous steady state.

A slightly different hyperbolic model with density-dependent speeds ($\gamma^+ = \gamma^+(u^+, \partial u^+/\partial x)$ and $\gamma^- = \gamma^-(u^-, \partial u^-/\partial x)$) and turning rates ($\lambda^+ = \lambda^- = \lambda(u^+, u^-)$) was introduced by Lutscher [47]:

$$\frac{\partial u^+}{\partial t} + \frac{\partial(u^+ \gamma^+(u^+, \partial u^+/\partial x))}{\partial x} = -\lambda(u^+, u^-)u^+ + \lambda(u^+, u^-)u^-, \quad (4.22a)$$

$$\frac{\partial u^-}{\partial t} - \frac{\partial(u^- \gamma^-(u^-, \partial u^-/\partial x))}{\partial x} = \lambda(u^+, u^-)u^+ - \lambda(u^+, u^-)u^-. \quad (4.22b)$$

The speeds γ^\pm depend not only on the local density of individuals, but also on the gradient of this density. In particular, these speeds satisfy the following additional elliptic equations

$$\beta \frac{\partial^2 \gamma^+}{\partial x^2} = \gamma^+ - E(u^+, \frac{\partial u^+}{\partial x}), \quad \beta \frac{\partial^2 \gamma^-}{\partial x^2} = \gamma^- - E(u^-, -\frac{\partial u^-}{\partial x}), \quad (4.23)$$

where E describes an expected speed. If this expected speed is constant (i.e., $E = \gamma$), then the speed of the individuals is also constant ($\gamma^\pm = \gamma$). Analytical results were used to discuss the stability of spatially homogeneous steady states. Numerical simulations were performed only for right-moving individuals, with the speed satisfying a parabolic equation of the form

$$\tau \frac{\partial \gamma^+}{\partial t} = \beta \frac{\partial^2 \gamma^+}{\partial x^2} - \gamma + E(u^+, \frac{\partial u^+}{\partial x}). \quad (4.24)$$

The results showed that model (4.22)–(4.24) can exhibit travelling pulse solutions.

The density-dependent speeds could also be the result of indirect interactions among organisms. These indirect interactions can be mediated by signals S produced by the organisms themselves: $\gamma^\pm = \gamma(S, \frac{\partial S}{\partial t}, \frac{\partial S}{\partial x})$, where S satisfies Eq. (4.7c) [27]. These signals could also be produced by other sources not investigated explicitly. Such a situation is common in tumour immunology, where the tumour-immune interactions are mediated by cytokines produced by various types of immune cells, not all of them being investigated in the models (see, for example, the tumour-immune interactions discussed in [48]). Mathematically, this situation could be modelled by incorporating into Eq. (4.7c) an external source of

communication signals. In Chap. 5 we will discuss a nonlocal model that considers such an approach.

A different situation that could be modelled by density-dependent speeds is the interaction of multiple species, each species influencing directly the velocity of the other species. To our knowledge, this “cross-advection” mechanism has not received much attention in the context of hyperbolic systems (although it has been recently investigated in parabolic models for population dynamics [49]). To model such a situation, the individuals’ speed would be described by $\gamma^\pm(u^\pm, v^\pm)$, where u^\pm and v^\pm are the two species. More generally, each species could produce signals S that would influence indirectly the speed of the other species: $\gamma^\pm(S(u^\pm, v^\pm))$.

Finally we note that the organisms’ velocities could also depend on their age (a) as well as their location in space (x): $\gamma = \gamma(a, x)$ [20]. We will revise this aspect in the next section, in the context of reaction hyperbolic systems.

We conclude this discussion on density-dependent speeds, by mentioning that in Sect. 5.8 we will consider a more general situation where the speed of individuals depends on the density of neighbours located further away (i.e., nonlocal speeds).

4.6 Models that Include Reaction Terms

When the hyperbolic models describe the evolution of organisms over long periods of time, they incorporate also population dynamics (i.e., birth and death processes). In this case, one has to be careful when modelling the death terms, since the left- and right-moving particles (organisms) die as left- and right-moving particles (organisms). On the other hand, the newly formed particles (organisms) can be either left-moving or right-moving. For detailed discussions of such models see [19, 20, 50–53]. The general equations for reaction-transport models with population dynamics are

$$\frac{\partial u^+}{\partial t} + \gamma \frac{\partial u^+}{\partial x} = -\lambda^+ u^+ + \lambda^- u^- + \frac{1}{2} m(u) u - g(u) u^+, \quad (4.25a)$$

$$\frac{\partial u^-}{\partial x} - \gamma \frac{\partial u^-}{\partial x} = \lambda^+ u^+ - \lambda^- u^- + \frac{1}{2} m(u) u - g(u) u^-. \quad (4.25b)$$

Here $u = u^+ + u^- \in \mathbb{R}$ is the total density, $m(u)$ models the production (multiplication) of particles/individuals/cells, and $g(u)$ models the death of these particles/individuals/cells. Note that while the production term depends on the total density u (and the new-born particles/individuals/cells become left-moving or right-moving with similar probabilities 1/2), the death terms depend on u^+ and u^- . These equations have been used, for example, to study animal dispersal [19], or to model epidemiological problems when the movement of infected individuals can be described by a correlated random walk process [20, 54].

Solutions for the reaction-transport system (4.25) have been investigated extensively: from existence and uniqueness results [24, 55, 56], to asymptotic behaviour

of solutions [56, 57] and invariance results [51]. System (4.25) was also shown to exhibit travelling front solutions [19, 20, 53, 56, 58, 59]. The minimal speed of the travelling fronts was proven to depend on the nonlinear functions $m(u)$ and $g(u)$ [58, 59].

The reaction-transport models (4.25) can be further generalised by adding density-dependent speeds ($\gamma(u)$) and turning rates ($\lambda^\pm(u)$) [60, 61]. Such models had been shown to exhibit travelling front solutions [61].

Finally, these reaction-transport models could be used to study populations structured by location in space (x) and age ($a \geq 0$) [20], or by some other internal state (especially relevant in case of cells, where signalling pathways inside cells influence cells' movement) [62]. For example, in [20] the authors assumed that age can influence the speed (γ) as well as the turning rates (λ^\pm) of organisms:

$$\frac{\partial u^+}{\partial t} + \frac{\partial u^+}{\partial a} + \frac{\partial \gamma(a, x) u^+}{\partial x} = -\lambda^+(a) u^+ + \lambda^-(a) u^- + \frac{1}{2} m(u) u - g(u) u^+, \quad (4.26a)$$

$$\frac{\partial u^-}{\partial x} + \frac{\partial u^-}{\partial a} - \frac{\partial \gamma(a, x) u^-}{\partial x} = \lambda^+(a) u^+ - \lambda^-(a) u^- + \frac{1}{2} m(u) u - g(u) u^-. \quad (4.26b)$$

Here, $u^\pm(a, x, t)$ describes the density of left- and right-moving individuals of age a , positioned at $x \in \mathbb{R}$ at time $t \in \mathbb{R}^+$. In contrast to the nonlocal birth term in model (3.30), here the birth rate does not depend explicitly on age.

In the context of bacterial colonies, Xue et al. [62] considered a hyperbolic model for the movement of an *E. coli* bacterial population, coupled with parabolic equations for the dynamics of chemicals consumed (i.e., aspartate $S(x, t)$) and secreted (i.e., succinate $F(x, t)$) by cells, and ordinary differential equations for the dynamics of internal cell variables. The density of left-moving and right-moving bacterial population is described by functions $u^\pm(x, \mathbf{y}, \mathbf{z}, t)$. Here $[\mathbf{y}, \mathbf{z}]$ is an internal state with variable \mathbf{y} describing signal transduction (where the coordinates $y_i, i = 1, \dots, q$, of this vector represent the concentrations of various proteins in the cell and receptor states involved in signal transduction) and variable \mathbf{z} describing cellular metabolism (where the coordinates $z_i, i = 1, 2$ include the concentration of the components in the TCA cycle and ATP). The equations for the evolution of the internal variables $\mathbf{y} = (y_1, \dots, y_q)$ and $\mathbf{z} = (z_1, z_2)$ are [62]:

$$\frac{dy_i}{dt} = \mathbf{f}(y_i, S), \quad i = 1, \dots, q, \quad \text{and} \quad \mathbf{f} = (f_1, \dots, f_q), \quad (4.27)$$

$$\frac{dz_1}{dt} = g_1(\mathbf{z}, F), \quad \text{with} \quad g_1(\mathbf{z}, F) = \frac{F(x, t) - z_1}{t_f}, \quad (4.28)$$

$$\frac{dz_2}{dt} = g_2(\mathbf{z}, F), \quad \text{with} \quad g_2(\mathbf{z}, F) = \frac{z_1 - z_2}{t_m}. \quad (4.29)$$

Here t_f is the characteristic time scale for the generation of the metabolic variable z_1 (e.g., fumarate in the TCA cycle; it is measured in seconds), while t_m is the characteristic time scale for the generation of variable z_2 (e.g., associated with the starving state of bacteria; it is measured in tens of minutes).

The equations for cells' movement are [62]:

$$\begin{aligned} \frac{\partial u^+}{\partial t} + s \frac{\partial u^+}{\partial x} + \sum_{i=1}^q \frac{\partial}{\partial y_i} (f_i(\mathbf{y}, S)u^+) + \sum_{i=1}^2 \frac{\partial}{\partial z_i} (g_i(\mathbf{z}, F)u^+) \\ = \lambda(\mathbf{y})[-u^+ + u^-] + k(\mathbf{z}u^+), \end{aligned} \quad (4.30)$$

$$\begin{aligned} \frac{\partial u^-}{\partial t} - s \frac{\partial u^-}{\partial x} + \sum_{i=1}^q \frac{\partial}{\partial y_i} (f_i(\mathbf{y}, S)u^-) + \sum_{i=1}^2 \frac{\partial}{\partial z_i} (g_i(\mathbf{z}, F)u^-) \\ = \lambda(\mathbf{y})[u^+ - u^-] + k(\mathbf{z}u^-). \end{aligned} \quad (4.31)$$

It is assumed that bacteria travel with a constant speed s , and the turning frequency of bacteria depends on the signal transduction variable ($\lambda(\mathbf{y})$), while the proliferation rate depends on the metabolic variables ($k(\mathbf{z})$). Finally, the equations for the evolution of the two chemicals, aspartate (S) and succinate (F) are [62]:

$$\begin{aligned} \frac{\partial S}{\partial t} = D_S \frac{\partial^2 S}{\partial x^2} + \alpha F \int \int h(z_2)(u^+(\mathbf{y}, \mathbf{z}) + u^-(\mathbf{y}, \mathbf{z}))d\mathbf{y}d\mathbf{z} \\ - \beta S \int \int (1 - h(z_2))(u^+(\mathbf{y}, \mathbf{z}) + u^-(\mathbf{y}, \mathbf{z}))d\mathbf{y}d\mathbf{z} - \gamma S, \end{aligned} \quad (4.32)$$

$$\frac{\partial F}{\partial t} = D_F \frac{\partial^2 F}{\partial x^2} - \beta F \int \int h(z_2)(u^+(\mathbf{y}, \mathbf{z}) + u^-(\mathbf{y}, \mathbf{z}))d\mathbf{y}d\mathbf{z}, \quad (4.33)$$

where it was assumed that $\alpha, \beta > 0$, $\gamma \geq 0$ and $h(z_2)$ is an increasing function of z_2 (e.g., $h(z_2) = az_2$). It was shown in [62] that this complex 1D mathematical model exhibits global weak solutions. This analytical result was complemented by numerical simulations that have shown stationary aggregations (which were also very slowly diffusing), and travelling band solutions (i.e., travelling pulses or rotating waves). It should be noted that for the numerical simulations, the authors used zero-flux boundary conditions. The hyperbolic equations for bacterial movement were discretised using an upwind scheme combined with a Van Leer flux limiting approach to preserve the positivity of solutions. The diffusion terms were approximated with the help of a central difference scheme. The integral terms in Eqs. (4.32)–(4.33) were discretised using a trapezoidal scheme. For more details regarding these numerical approaches, see Chap. 7.

The models discussed until now assumed that the individuals/particles/cells are moving either left (−) or right (+). However, in many situations it is possible to have also third state, where the individuals/particles/cells are not moving. Such a class of models was discussed in the review article by Bressloff and Newby [28],

in the context of active intracellular transport. Particles moving along a single microtubular filament (of length L) can be bound to the filament and moving left (u^-) or right (u^+), or can be unbound from the filament and (maybe) diffusing (u_0); see also Fig. 4.2. The equations describing the dynamics of these different types of particles could be written as follows:

$$\frac{\partial u^+}{\partial t} + v \frac{\partial u^+}{\partial x} = -\beta^+ u^+ + \alpha u_0, \quad (4.34a)$$

$$\frac{\partial u^-}{\partial t} - v \frac{\partial u^-}{\partial x} = -\beta^- u^- + \alpha u_0, \quad (4.34b)$$

$$\frac{\partial u_0}{\partial t} = D_0 \frac{\partial^2 u_0}{\partial x^2} + \beta^+ u^+ + \beta^- u^- - 2\alpha u_0. \quad (4.34c)$$

In the above equations $v \in \mathbb{R}^+$ is the speed of bound left-moving/right-moving particles, D_0 is the diffusion rate of unbound particles, while $\beta^\pm \in \mathbb{R}^+$ and $\alpha \in \mathbb{R}^+$ are the transition rates between the moving and stationary states. Note that in this model a filament-bound left-moving particle can become right-moving only after becoming stationary and unbound (i.e., there is no direct transition between $u^- \leftrightarrow u^+$, and so the reaction terms are slightly different from those in the models above). Since this model was defined on a finite domain $[0, L]$, boundary conditions were included in the model description: for example, a reflecting boundary at $x = 0$ (i.e., $u^-(0, t) = u^+(0, t)$), and an absorbing boundary at $x = L$ (i.e., $u^-(L, t) = 0$) [28].

This class of models (with/without diffusion for u_0 and even for u^\pm) for motor-assisted transport of particles along microtubules/axons have been investigated analytically and numerically in terms of: finding exact analytical solutions (using Laplace transforms) [63–65], showing the existence of travelling waves [66], performing numerical simulations for the time-evolution of solutions [63, 65, 67, 68]. Some studies even compared the numerical simulated solutions with experimental data [67, 68].

4.7 Traffic Models

4.7.1 First-Order Models

Local hyperbolic systems are also used to model traffic or pedestrian flows characterised by two distinct velocities $\gamma_{1,2} \in \mathbb{R}$. However, in this case, the “reaction” terms are actually speed-adaptation terms. A two-velocity model was first introduced by Ruijgrok and Wu [69] in the context of gas dynamics:

$$\frac{\partial u^+}{\partial t} + \gamma_1 \frac{\partial u^+}{\partial x} = -\alpha u^+ + \beta u^- + \mu u^+ u^-, \quad (4.35a)$$

$$\frac{\partial u^-}{\partial t} + \gamma_2 \frac{\partial u^-}{\partial x} = \alpha u^+ - \beta u^- - \mu u^+ u^-, \quad (4.35b)$$

As opposed to the models in the previous section, where the two velocities were $\gamma_1 = -\gamma_2$, here both velocities $\gamma_{1,2}$ could be positive. The last terms on the right-hand-side of Eqs. (4.35) describe the transition from velocity γ_2 to velocity γ_1 following a binary collision with intensity μ . If $\gamma_2 > \gamma_1$, these terms model the slowing-down process that takes place when a car of velocity γ_2 travels behind a car with velocity γ_1 .

A different class of multi-equation models describes the heterogeneous traffic exhibited by multi-groups of drivers (i.e., cars, trucks, or vehicles with different trips [70]). These types of models (see, for example, [71, 72]) denote by $u_i(t, x)$, $i = 1, \dots, n$, the density of vehicles in the i -th class of drivers, and by $v_i(u_1, \dots, u_n)$ the average speed of the i -th class:

$$\frac{\partial u_i}{\partial t} + \frac{\partial(u_i v_i)}{\partial x} = 0, \quad i = 0, \dots, n. \quad (4.36)$$

As for single-population first-order models, the speed has the general form $v_i(u) = \psi(\bar{u})v_i^*$, with v_i^* the maximum speed for drivers in the i -th class, and $\psi(\bar{u})$ a decreasing function of the total population $\bar{u} = u_1 + \dots + u_n$, with $\psi(0) = 1$ (or some positive constant) and $\psi(u_{max}) = 0$ (with u_{max} the maximum possible density for the road) [70]. These types of models (with these assumptions on the speed variable) admit entropy admissible shock wave solutions [70, 72].

4.7.2 Second-Order Models

Similar to the one-population models, the two-population models (for the dynamics of left-moving/right-moving individuals) can be cast as second-order models by introducing explicit formulas for the velocity of left-moving and right-moving individuals. Appert-Roland et al.[45] introduced the following model for the movement of two pedestrian subpopulations $u^\pm \in \mathbb{R}$ on one lane:

$$\frac{\partial u^+}{\partial t} + \frac{\partial(u^+ v^+)}{\partial x} = 0, \quad (4.37a)$$

$$\frac{\partial u^-}{\partial t} + \frac{\partial(u^- v^-)}{\partial x} = 0, \quad (4.37b)$$

$$\frac{\partial(u^+ w^+)}{\partial t} + \frac{\partial(u^+ w^+ v^+)}{\partial x} = 0, \quad (4.37c)$$

$$\frac{\partial(u^- w^-)}{\partial t} + \frac{\partial(u^- w^- v^-)}{\partial x} = 0, \quad (4.37d)$$

$$w^+ = v^+ + p(u^+, u^-), \quad (4.37e)$$

$$w^- = -v^- + p(u^-, u^+). \quad (4.37f)$$

As mentioned in Chap. 3, where we discussed a similar one-population model, $(v^+, v^-) \in \mathbb{R}^+ \times \mathbb{R}^-$ describe the actual velocities for the two populations (with $v^+ > 0$ for right-moving individuals and $v^- < 0$ for left-moving individuals), while $(w^+, w^-) \in \mathbb{R}^+ \times \mathbb{R}^+$ describe the desired pedestrian velocities in the absence of any obstacles. Because the offset velocities $p(u^\pm, u^\mp) > 0$ can be very large (since p is not bounded; see Chap. 3), the actual velocities can reverse their sign. This way, under the pressure of large right-moving (left-moving) crowds, the left-moving (right-moving) individuals will reverse direction and will follow the majority of the population, thus leading to the formation of travelling pulses. The model can be easily generalised to consider congestion dynamics: $u^\pm \rightarrow u_\epsilon^\pm$, $w^\pm \rightarrow w_\epsilon^\pm$, $v^\pm \rightarrow v_\epsilon^\pm$ and $p(u^\pm, u^\pm) \rightarrow p^\epsilon(u_\epsilon^\pm, u_\epsilon^\mp)$, with p^ϵ described by (4.21).

Model (4.37) can be further generalised to describe the movement of pedestrians via multiple lanes. Thus, if one denotes by k the lane index, $k = 1, 2, \dots, K < \infty$, then the model reads [45]:

$$\frac{\partial u_k^+}{\partial t} + \frac{\partial(u_k^+ v_k^+)}{\partial x} = S_k^+, \quad (4.38a)$$

$$\frac{\partial u_k^-}{\partial t} + \frac{\partial(u_k^- v_k^-)}{\partial x} = S_k^-, \quad (4.38b)$$

$$\frac{\partial(u_k^+ w_k^+)}{\partial t} + \frac{\partial(u_k^+ w_k^+ v_k^+)}{\partial x} = R_k^+, \quad (4.38c)$$

$$\frac{\partial(u_k^- w_k^-)}{\partial t} + \frac{\partial(u_k^- w_k^- v_k^-)}{\partial x} = R_k^-, \quad (4.38d)$$

$$w_k^+ = v_k^+ + p_k(u_k^+, u_k^-), \quad (4.38e)$$

$$w_k^- = -v_k^- + p_k(u_k^-, u_k^+). \quad (4.38f)$$

Here, S_k^\pm and R_k^\pm are source terms that model the transition rates between different lanes. Generally, pedestrians change lanes from k to $k \pm 1$. In [45] the authors denoted by $\lambda_{k \rightarrow k \pm 1}^+$ and $\lambda_{k \rightarrow k \pm 1}^-$ the transition rates for right-moving and left-moving pedestrians, and assumed that $\lambda_{k \rightarrow k \pm 1}^\pm$ are decreasing with $u_{k \pm 1} = u_{k \pm 1}^+ + u_{k \pm 1}^-$, while the rates are zero at congestion: $u_{k \pm 1} = u^*$. With these assumptions, the transition rates can be written as:

$$S_{k,\alpha} = \lambda_{k+1 \rightarrow k}^\alpha u_{k+1}^\alpha + \lambda_{k-1 \rightarrow k}^\alpha - (\lambda_{k \rightarrow k+1}^\alpha + \lambda_{k \rightarrow k-1}^\alpha) u_k^\alpha, \quad (4.39a)$$

$$R_k^\pm = \lambda_{k+1 \rightarrow k}^\alpha u_{k+1}^\alpha w_{k+1}^\alpha + \lambda_{k-1 \rightarrow k}^\alpha u_{k-1}^\alpha w_{k-1}^\alpha - (\lambda_{k \rightarrow k+1}^\alpha + \lambda_{k \rightarrow k-1}^\alpha) u_k^\alpha w_k^\alpha, \quad (4.39b)$$

$$\alpha = \pm. \quad (4.39c)$$

Note that model (4.38) does not actually describe the spontaneous segregation of pedestrians into different lanes. It only describes pedestrian dynamics after the

lanes are formed. Unfortunately, the authors in [45] do not present any numerical simulations for these multi-lane models.

4.8 Multiple Population Models

In contrast to the models presented in the previous section (which described the dynamics of one population formed of left-moving/right-moving individuals travelling on one lane (4.37) or on different lanes (4.38)), we now consider the case of multiple populations moving through a one-lane domain. To this end, we generalise models (4.3)–(4.25) to multiple species by considering a vector $u^\pm = [u_i^\pm] \in \mathbb{R}^n$, $i = 1..n$ [20, 26]. Here, u_i^\pm denotes the left-moving (–) and right-moving (+) particles of species i . Such models have been used to investigate typical species interactions, such as predator-prey, competition, or mutualism [20], Turing aggregation patterns [52], as well as epidemics spread [54].

As an example, Lutscher and Stevens [26] introduced the following two-population model to describe the interactions between two cell types that differ in their turning behaviour (due to different inter-cellular signalling):

$$\frac{\partial u_1^+}{\partial t} + \gamma \frac{\partial u_1^+}{\partial x} = -(\mu + \lambda^+)u_1^+ + (\mu + \lambda^-)u_1^-, \quad (4.40a)$$

$$\frac{\partial u_1^-}{\partial t} - \gamma \frac{\partial u_1^-}{\partial x} = (\mu + \lambda^+)u_1^+ - (\mu + \lambda^-)u_1^-, \quad (4.40b)$$

$$\frac{\partial u_2^+}{\partial t} + \gamma \frac{\partial u_2^+}{\partial x} = -(\mu + v^+)u_1^+ + (\mu + v^-)u_1^-, \quad (4.40c)$$

$$\frac{\partial u_2^-}{\partial t} - \gamma \frac{\partial u_2^-}{\partial x} = (\mu + v^+)u_1^+ - (\mu + v^-)u_1^-, \quad (4.40d)$$

where $\mu \geq 0$ is a constant turning rate and $\lambda^\pm(u_1^\pm, u_2^\pm)$ and $v^\pm(u_1^\pm, u_2^\pm)$ are the density-dependent turning rates that result from cell-cell interactions. The authors also assumed various symmetry conditions in regard to the turning rates (conditions that affect also the symmetry of the entire system):

$$\lambda^\pm(u_1^+, u_1^-, u_2^+, u_2^-) = \lambda^\pm(u_1^+, u_1^-, u_2^-, u_2^+), \quad (4.41a)$$

$$v^\pm(u_1^+, u_1^-, u_2^+, u_2^-) = v^\pm(u_1^+, u_1^-, u_2^-, u_2^+), \quad (4.41b)$$

$$v^+(u_1^+, u_1^-) = v^-(u_1^-, u_1^+), \quad (4.41c)$$

The authors in [26] investigated the stability of the spatially homogeneous steady states $u_1^\pm = c_1$ and $u_2^\pm = c_2$, and showed analytically that at the bifurcation point all eigenvalues cross the imaginary axis. Thus, the instability arises via a Hopf bifurcation. Although the model likely displays rotating waves (i.e., travelling

pulses—as a result of Hopf bifurcations), no numerical simulations were presented to confirm the type of patterns obtained with model (4.40).

A somehow similar two-population model was introduced by Watmough and Edelstein-Keshet [73] to describe the dynamics of ant leaders/pioneers and followers, in response to the density of a pheromone trail. However, in contrast to the model in [26], here the hyperbolic equations for the dynamics of left-moving and right-moving leaders (L^\pm) and right-moving and left-moving followers (F^\pm), are coupled with an ODE for the degradation and production of pheromones (T):

$$\begin{aligned} \frac{\partial T(x, t)}{\partial t} &= -\gamma T(x, t) + \tau_f F(x, t) + \tau_l L(x, t), \quad \text{with} \\ F &= F^+ + F^-, \quad L = L^+ + L^-, \end{aligned} \quad (4.42)$$

and

$$\frac{\partial F^+}{\partial t} + v \frac{\partial F^+}{\partial x} = -\epsilon F^+ + \alpha L^+ T - \rho^+ F^+ + \rho^- F^-, \quad (4.43a)$$

$$\frac{\partial F^-}{\partial t} - v \frac{\partial F^-}{\partial x} = -\epsilon F^- + \alpha L^- T + \rho^+ F^+ - \rho^- F^-, \quad (4.43b)$$

$$\frac{\partial L^+}{\partial t} + s \frac{\partial L^+}{\partial x} = \epsilon F^+ - \alpha L^+ T - \lambda L^+ + \lambda L^-, \quad (4.43c)$$

$$\frac{\partial L^-}{\partial t} - s \frac{\partial L^-}{\partial x} = \epsilon F^- - \alpha L^- T + \lambda L^+ - \lambda L^-. \quad (4.43d)$$

In the pheromone equation (4.42) γ is the degradation rate, while τ_f and τ_l are the production rates. In Eqs. (4.43) for the ants movement, λ and ρ^\pm describe the turning rates, s and v are the speeds of leaders and followers, while ϵ and α describe the exchanges between leaders and followers. Note that the pheromone density acts as a communication mechanisms between leaders and followers (with leaders becoming followers, at a rate αT , when they encounter and follow the pheromone trails). The authors reduced this 5-equation system to a 3-equation system for the total follower (F) and leader (L) populations, and the density T of pheromones. Then they studied the stability of the spatially-homogeneous steady states displayed by the reduced model, and used the results to show qualitatively the existence of travelling waves as heteroclinic orbits connecting the steady states. Numerical simulations confirmed the existence of these travelling waves.

We decided to present this model for ants movement along pheromone trails, as a simple example of local communication between different populations via a chemical produced by the members of both populations. In contrast to the model by Hillen and Stevens [27] discussed above, where the turning rates depended also on the gradient of the external chemical (thus suggesting nonlocal interactions via the chemical signal, among the members of the same population), in model (4.43) the interactions between the two populations depend on the local density of

the chemical. In the next chapter we will discuss more complex communication mechanisms, which can lead to short-range and/or long-range interactions among individuals (i.e., repulsion, attraction and alignment). In that context, we will return to the investigation of multiple populations which use different animal communication mechanisms to interact with each other. Furthermore, in Chap. 6 we will discuss another model for ant-trail formation through pheromone deposition, where the pheromone sensing will be assumed nonlocal.

Remark 4.4 The local hyperbolic models presented in these last two chapters form the basis of modelling directional movement in animal/human communities. Moreover, the majority of models presented here were simple enough to be amenable to analytical and numerical investigation of the solutions. However, the approaches taken in these studies did not identify a large variety of patterns displayed by these local models. It is not clear whether this is the result of an insufficient investigation of the parameter spaces for these local models, or the models themselves cannot exhibit more exotic patterns (due to their bifurcation and symmetry structure). In the next two chapters, the focus will be on hyperbolic/kinetic models that include nonlocal interactions between conspecifics. Particular emphasis will be on the complex types of patterns that can be displayed by these nonlocal models. This way, we aim to emphasise the contribution of nonlocal interactions (as a result of nonlocal animal-animal and cell-cell communication) to the complex behaviours observed in animal and cell aggregations.

Remark 4.5 Since many of the models discussed above have been derived using random walk approaches, they incorporate intrinsically various stochastic aspects (e.g., random initial positions of particles, transitions between moving/stationary states governed by Markov processes, etc.; Note that a Markov process is a stochastic process in which the future is independent of the past, given that we know the present [74]). For a more in-depth discussion of stochastic processes in relation to transport equations in cell biology, we refer the reader to [28, 75]. We will return to the aspect of stochasticity at the end of Chap. 5, where we will discuss the explicit incorporation of environmental noise into hyperbolic/kinetic models for collective dynamics.

References

1. A. Zienkiewicz, D. Barton, M.D. Bernardo, Eur. Phys. J. Spec. Top. **224**, 3343 (2015)
2. V. Mwaffo, S. Butail, M. di Bernardo, M. Porfiri, Zebrafish **12**(3), 250 (2015)
3. J. Killen, H. Thurfjell, S. Ciuti, D. Paton, M. Musiani, M. Boyce, Mov. Ecol. **2**(1), 15 (2014)
4. T. Yang, J.S. Park, Y. Choi, W. Choi, T.W. Ko, K. Lee, PLoS ONE **6**(6), e20255 (2011)
5. C. Qian, C. Wong, S. Swarup, K.H. Chiam, Appl. Environ. Microbiol. **79**(15), 4734 (2013)
6. A. Patterson, A. Gopinath, M. Goulian, P. Arratia, Sci. Rep. **5**, 15761 (2015)
7. S. Yazdi, A. Ardekani, Biomicrofluidics **6**, 044114 (2012)
8. R. Stocker, Proc. Natl. Acad. Sci. USA **108**(7), 2635 (2011)
9. L. Xie, T. Altindal, S. Chattopadhyay, X.L. Wu, Proc. Natl. Acad. Sci. USA **105**, 4209 (2011)

10. M. Segal, I. Soifer, H. Petzold, J. Howard, M. Elbaum, O. Reiner, *Biol. Open* **1**, 1–12 (2012)
11. E. Reese, L. Haimo, *J. Cell Biol.* **151**, 155 (2000)
12. M. Müller, S. Klumpp, R. Lipowsky, *Proc. Natl. Acad. Sci.* **105**(12), 4609 (2008)
13. M. Welte, *Curr. Biol.* **14**, R525 (2004)
14. A. John, A. Schadschneider, D. Chowdhury, K. Nishinari, *J. Theor. Biol.* **231**(2), 279 (2004)
15. W. Alhajyaseen, H. Nakamura, M. Asano, *Proc. Soc. Behav. Sci.* **16**, 526 (2011)
16. C. Feliciani, K. Nishinari, *Phys. Rev. E* **94**, 032304 (2016)
17. S. Goldstein, *Quart. J. Mech. Appl. Math.* **4**, 129 (1951)
18. M. Kac, *Rocky Mt. J. Math.* **4**, 497 (1974)
19. E.E. Holmes, *Am. Nat.* **142**, 779 (1993)
20. K. Hadel, Reaction transport systems in biological modelling, in *Mathematics Inspired by Biology*. Lecture Notes in Mathematics (Springer, Berlin, 1999), pp. 95–150
21. E. Codling, M. Plank, S. Benhamou, *J. R. Soc. Interface* **5**(25), 813 (2008)
22. D. Grünbaum, A. Okubo, in *Frontiers in Mathematical Biology*, ed. by S.A. Levin. Lecture Notes in Biomathematics, vol. 100 (Springer, Berlin, 1994), pp. 296–325
23. M.A. Lewis, *Theor. Popul. Biol.* **45**, 277 (1994)
24. T. Hillen, *Can. Appl. Math. Q.* **18**(1), 1 (2010)
25. H. Hasimoto, *Proc. Jpn. Acad. Ser. A Math. Sci.* **50**, 623 (1974)
26. F. Lutscher, A. Stevens, *J. Nonlinear Sci.* **12**, 619 (2002)
27. T. Hillen, A. Stevens, *Nonlinear Anal.: Real World Appl.* **1**, 409 (2000)
28. P. Bressloff, J. Newby, *Rev. Mod. Phys.* **85**(1), 135 (2013)
29. F. Lutscher, *J. Math. Biol.* **45**, 234 (2002)
30. L.A. Segel, *SIAM J. Appl. Math.* **32**, 653 (1977)
31. K. Kang, A. Scheel, A. Stevens, *ArXiv* (2018)
32. U. Börner, A. Deutsch, H. Reichenbach, M. Bär, *Phys. Rev. Lett.* **89**, 078101 (2002)
33. U. Börner, A. Deutsch, M. Bär, *Phys. Biol.* **3**, 138 (2006)
34. O. Igoshin, A. Mogilner, R. Welch, D. Kaiser, G. Oster, *Proc. Natl. Acad. Sci. USA* **98**, 14913 (2001)
35. O.A. Igoshin, R. Welch, D. Kaiser, G. Oster, *Proc. Natl. Acad. Sci. USA* **101**, 4256 (2004)
36. O.A. Igoshin, G. Oster, *Math. Biosci.* **188**, 221 (2004)
37. R. Eftimie, G. de Vries, M.A. Lewis, *Proc. Natl. Acad. Sci. USA* **104**(17), 6974 (2007)
38. T. Hillen, H. Levine, *Z. Angew. Math. Phys.* **54**, 1 (2003)
39. Y.L. Chuang, M. D’Orsogna, D. Marthaler, A. Bertozzi, L. Chayes, *Phys. D* **232**, 33 (2007)
40. A. Scheel, A. Stevens, *J. Math. Biol.* **75**, 1047 (2017)
41. J.R. Hunter, *Anim. Behav.* **17**, 507 (1969)
42. J. Bick, G. Newell, *Q. Appl. Math.* **18**, 191 (1960)
43. A. Chertock, A. Kurganov, A. Polizzi, I. Timofeyev, *Math. Models Methods Appl. Sci.* **81**, 1947 (2003)
44. A. Kurganov, C.T. Lin, *Commun. Comput. Phys.* **2**, 141 (2007)
45. C. Appert-Rolland, P. Degond, S. Motch, *Netw. Heterog. Media* **6**(3), 351 (2011)
46. A. Kurganov, E. Tadmor, *J. Comput. Phys.* **160**, 240 (2000)
47. F. Lutscher, *Eur. J. Appl. Math.* **14**, 291 (2003)
48. R. Eftimie, J. Bramson, D. Earn, *J. Theor. Biol.* **265**, 467 (2010)
49. E. Zenskova, K. Kassner, M. Tsyganov, M. Hauser, *Eur. Phys. J. B.* **72**, 457 (2009)
50. K. Hadel, *Math. Comput. Model.* **31**(4–5), 75 (2000)
51. T. Hillen, *J. Math. Anal. Appl.* **210**, 360 (1997)
52. T. Hillen, *J. Math. Biol.* **35**, 49 (1996)
53. K. Hadel, *Can. Appl. Math. Q.* **2**, 27 (1994)
54. K. Hadel, in *Proceedings of the Thirteenth Dundee Conference*, ed. by R. Jarvis (1996), pp. 18–32
55. T. Hillen, Nichtlineare hyperbolische systeme zur modellierung von ausbreitungsvorgängen und anwendung auf das turing modell. Ph.D. thesis, Universität Tübingen, 1995
56. D. Needham, J. Leach, *IMA J. Appl. Math.* **73**, 158 (2008)

57. T. Hillen, Qualitative analysis of hyperbolic random walk systems. Technical report, SFB 382, Report No. 43, 1996
58. K. Hadeler, Nonlinear propagation in reaction transport systems, in *Differential Equations with Applications to Biology*. Fields Institute Communications (American Mathematical Society, Providence, 1998), pp. 251–257
59. K. Hadeler, *J. Math. Sci.* **149**(6), 1658 (2008)
60. K. Hadeler, Reaction-telegraph equations with density-dependent coefficients, in *Partial Differential Equations. Models in Physics and Biology*. Mathematical Research, vol. 82 (Akademie-Verlag, Berlin, 1994), pp. 152–158
61. K. Hadeler, in *Differential Equations and Applications to Biology and Industry. Proceedings of the Claremont International Conference*, ed. by M. Martelli, K. Cooke, E. Cumberbatch, B. Tang, H. Thieme (1996), pp. 145–156
62. C. Xue, H. Hwang, K. Painter, R. Erban, *Bull. Math. Biol.* **73**, 1695 (2011)
63. A. Kuznetsov, A.A. Avramenko, *Proc. R. Soc. A* **464**, 2867 (2008)
64. A. Kuznetsov, *Proc. R. Soc. A* **468**, 3384 (2012)
65. I. Kuznetsov, A. Kuznetsov, *J. Biol. Phys.* **40**, 41 (2014)
66. A. Friedman, G. Craciun, *SIAM J. Math. Anal.* **38**(3), 741 (2006)
67. P. Jung, A. Brown, *Phys. Biol.* **6**(4), 046002 (2009)
68. P. Monsma, Y. Li, J. Fenn, P. Jung, A. Brown, *J. Neurosci.* **34**(8), 2979 (2014)
69. T. Ruijgrok, T. Wu, *Phys. A* **113**, 401 (1982)
70. M. Garavello, B. Piccoli, *Netw. Heterog. Media* **4**(1), 107 (2009)
71. G. Wong, S. Wong, *Transp. Res. A* **36**, 827 (2002)
72. S. Benzoni-Gavage, R. Colombo, *Eur. J. Appl. Math.* **14**, 587 (2003)
73. J. Watmough, L. Edelstein-Keshet, *J. Math. Biol.* **33**, 459 (1995)
74. E. Dynkin, *Markov Processes*. Die Grundlehren der Mathematischen Wissenschaften (In Einzeldarstellungen mit Besonderer Berücksichtigung der Anwendungsgebiete), vol. 121/122 (Springer, Berlin, 1965)
75. P. Bressloff, *Stochastic Processes in Cell Biology* (Springer, Cham, 2014)